

Anomalous diffusion and stress relaxation in surfactant micelles

Subas Dhakal*

Department of Biomedical and Chemical Engineering, Syracuse University, Syracuse, New York 13244, USA

Radhakrishna Sureshkumar†

*Department of Biomedical and Chemical Engineering, Syracuse University, Syracuse, New York 13244, USA
and Department of Physics, Syracuse University, Syracuse, New York 13244, USA*

(Received 4 November 2016; published 24 July 2017)

We investigate the mechanisms of anomalous diffusion in cationic surfactant micelles using molecular dynamics simulations in the presence of explicit salt and solvent-mediated interactions. Simulations show that when the counterion density increases, saddle-shaped branched interfaces manifest. In experiments, branched structures exhibit lower viscosity as compared to linear and wormlike micelles. This has long been attributed to stress relaxation arising from the sliding motion of branches along the main chain. Our simulations reveal a mechanism of branch motion resulting from an enhanced counterion condensation at the branched interfaces and provide quantitative evidence of stress relaxation facilitated by branched sliding. Furthermore, depending on the surfactant and salt concentrations, which in turn determine the microstructure, we observe normal, subdiffusive, and superdiffusive motions of surfactants. Specifically, superdiffusive behavior is associated with branch sliding, breakage and recombination of micelle fragments, as well as constraint release in entangled systems.

DOI: [10.1103/PhysRevE.96.012605](https://doi.org/10.1103/PhysRevE.96.012605)**I. INTRODUCTION**

Over the past decades, the structure, dynamics, and mechanical properties of self-assembled aggregates of cationic surfactants have been studied extensively [1–21]. Self-assembly of cationic surfactant solutions can be controlled by manipulating the solvent-mediated electrostatic interactions among the surfactant molecules by altering the counterion concentration. A rich variety of fluctuating micelle morphologies can thus be formed, such as spheres, cylinders, wormlike chains, as well as branched and loopy structures [8–10,12]. The aggregate shape, which depends on the solution temperature as well as the concentrations of the surfactant and the counterion, has a profound effect on the rheological properties of micelle solutions. Both experiments and recent simulations [8–10] have shown the existence of branched structures in ionic surfactant solutions. It has been hypothesized that, unlike in branched polymers, thermal fluctuations can cause micelle branches to slide along the contour of the main chain and thereby provide an additional mechanism of stress relaxation [9,11,20,21]. Electrostatic screening by counterions is known to promote branch formation and an accompanying reduction in the solution viscosity [8,11]. Despite the extensive literature on branched micelle systems, two major questions regarding their structure and dynamics remain unanswered:

(i) *Mechanisms and energetics of branching.* Branched structures are formed in a cationic surfactant solution as the salinity is increased [8–11]. However, the physical mechanisms underlying their formation are unclear. Second, in this paper we perform direct molecular-level visualizations to study the energetics of branched structures. Third, direct evidence of branch sliding and its influence on stress relaxation are lacking in the literature. Quantifying such putative motions of

micelle branches poses a great challenge to experiments and molecular simulations. In this paper, we address the above mentioned questions via coarse-grained molecular dynamics (CGMD) simulations of cationic surfactant micelle solutions of cetyl-trimethyl-ammonium chloride (CTAC) in the presence of a binding organic salt sodium salicylate (NaSal), a widely used system in experiments [3–5,11].

(ii) *Anomalous diffusion.* Anomalous diffusion is ubiquitous in many phases of soft condensed matter. Subdiffusive behavior is encountered in crowded systems due to topological constraints, e.g., the reptative motion of polymer chains in an entangled polymer melt. On the other hand, superdiffusion is less common. Examples include molecular diffusion in glass forming liquids [22], microscale particle diffusion in bacterial suspensions [23], and spin transport in Heisenberg quantum magnets [24]. Wormlike micelle solutions exist in a dynamic equilibrium determined by breakage and recombination events and are inherently polydisperse. Such dynamics and entanglement effects can cause large variations in the mobility of individual surfactants within the system [17,18]. For instance, the lifetime of trapping due to entanglements would depend on the micelle length, and hence the motion of individual surfactant molecules could vary from one aggregate to the other. In fact, Ott *et al.* [18] observed anomalous self-diffusion of surfactants in a solution of cetyl trimethyl bromide by measuring the diffusion of fluorescent probes using the fringe-pattern photobleaching (FRAP) technique. In this technique, the self-diffusion coefficient is measured by tracking fluorescence probe molecules which are similar to the cetyl-trimethyl-ammonium bromide (CTAB) molecules and have the ability to associate with CTAB micelles. Specifically, the mean-square displacement (MSD) of the probe molecules was found to scale as $\langle [\vec{r}(t) - \vec{r}(0)]^2 \rangle \sim t^\beta$ with $\beta \neq 1$. For times shorter than the reptation time ($t \leq \tau_r$), superdiffusive behavior often was observed whereas subdiffusive behavior was more common for $t \gg \tau_r$. On the other hand, normal ($\beta = 1$) and subdiffusive ($\beta \leq 1$) behaviors were observed in

*sdhakalsnu@gmail.com

†rsureshk@syr.edu

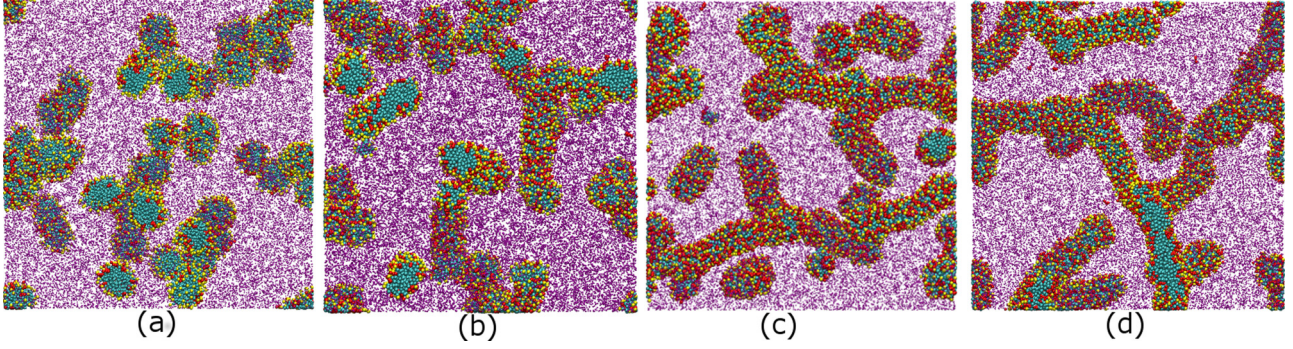


FIG. 1. Snapshots from simulations depicting the microstructure at the surfactant concentration of $c_D = 0.1 M$ and various salt to surfactant ratios (R): (a) $R = 0.2$, (b) $R = 0.4$, (c) $R = 0.6$, and (d) $R = 0.8$. Color scheme: red (Sal^-), yellow (hydrophilic part of the surfactant), and cyan (hydrocarbon tail). For the sake of clarity, water molecules are represented by purple dots in the background.

dilute solutions for long times. These authors attributed the superdiffusive motion to a *Levy flight*, a random walk with a long-tailed probability distribution of step sizes, caused by the reptation of shorter micelles. In this paper, we provide an analysis of surfactant motion at various salt (c_S) and surfactant (c_D) concentrations to understand the mechanisms of anomalous diffusion in CTAC-NaSal solutions.

II. COARSE-GRAINED MOLECULAR DYNAMICS SIMULATIONS

CGMD simulations of a model [6–8] of CTAC-NaSal solution in water are conducted using the LAMMPS [25] molecular dynamics package. This model utilizes the MARTINI force field [26] to represent the interactions among the CG beads. Coarse-grained representations of surfactant, salt, water, and ions can be found in our previous papers [6,8]. The nonbonded interaction between any two beads is described by a truncated Lennard-Jones potential,

$$V_{LJ}(r) = 4\epsilon \left[\left(\frac{\sigma}{r} \right)^{12} - \left(\frac{\sigma}{r} \right)^6 \right], \quad (1)$$

with the cutoff at $r = 1.2$ nm. Here r is the center-to-center distance between two beads, σ is the effective diameter, and ϵ is the depth of the potential well, respectively. The parameters σ and ϵ for different types of beads are defined in Ref. [26].

The connectivity between the bonded beads within the same molecule is modeled via a harmonic spring potential,

$$V_b(r) = \frac{K_b}{2}(r - r_0)^2. \quad (2)$$

Here $K_b = 1250 \text{ kJ mol}^{-1} \text{ nm}^{-2}$ is the spring constant. An equilibrium distance of $r_0 = 0.47$ nm is used for all bonds whereas those within the benzene ring of Sal^- are constrained at $r_0 = 0.27$ nm. The angle potential between three sequential beads is modeled via

$$V_a(r) = \frac{K_a}{2}(\cos \theta - \cos \theta_0)^2, \quad (3)$$

with the force constant of $K_a = 25 \text{ kJ mol}^{-1}$ and an equilibrium angle of $\theta_0 = 180$. Finally, the electrostatic potential between two beads with charges q_i and q_j is modeled via $\phi_{ij} = \frac{q_i q_j}{4\pi\epsilon_0\epsilon_r r}$ where ϵ_0 is the permittivity of the free space. The

relative dielectric constant of the medium is set to $\epsilon_r = 15$ [26]. A particle-particle particle-mesh solver is used to compute long-range electrostatic interactions. The equation of motion is integrated with a time step of $\Delta t = 15$ fs for a constant NVT ensemble with the temperature controlled via a Nosé-Hoover thermostat.

III. RESULTS AND DISCUSSION

We conduct MD simulations at $c_D = 0.1, 0.2, 0.3 M$ for various $R = c_S/c_D = 0.2, 0.4, 0.6, 0.8$ values to understand the mechanisms of branch formation and stress relaxation in micelles. The size of our simulation box is approximately 35 nm in each dimension and consists of approximately 5×10^5 CG beads including water, surfactants, salts, and ions (see the details in Ref. [8]). Snapshots from the simulations showing the microstructures at various values of R at a fixed surfactant concentration of $c_D = 0.1 M$ are displayed in Fig. 1. It clearly illustrates a gradual change from cylindrical and wormlike micelles to branched structures with increasing salt concentration.

A. Energetics of branched micelles

We present typical examples of micelle-water interfaces in Fig. 2 formed at different salt and surfactant concentrations. Specifically, surfaces with positive, zero, and negative Gaussian curvature K corresponding to spherical, cylindrical, and branched micelles with saddle-shaped junctions are observed. To understand the energetics of branch formation, we analyzed the counterion distribution in a typical *Y-shaped* branched structure shown in Fig. 2(c). We divided the micelle surface into patches of a radius of ~ 1 nm and calculated the effective charge Q by summing over the partial charges within the patch. We show the distribution of Q over the micelle surface in Fig. 3(a). Surfactant head groups color coded with the Q value on the surrounding patch are shown in Fig. 3(b). Three distinct regions can be observed, namely, spherical caps (S), cylindrical regions (C), and a saddle-shaped junction (B). We observe that the counterion density is the maximum in the B region, intermediate in the C region, and the least in the S region. At the saddle junction, surfactant orientations are aligned closely with the surface normal as shown schematically in Fig. 2(c). This

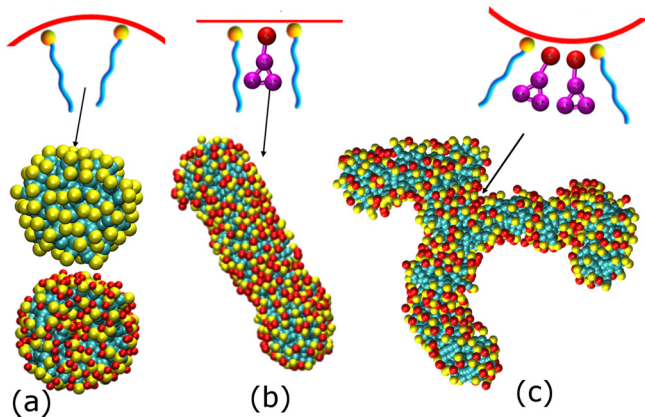


FIG. 2. Hydrophobic-water interfaces of micelles at $c_D = 0.2M$ with different Gaussian curvatures (K): (a) spherical, $K > 0$ [$R = 0$ (top), $R = 1.2$ (bottom)], (b) cylindrical ($R = 1.2$), $K = 0$, and (c) hyperbolic ($R = 1.2$), $K < 0$. Changes in the shape and curvature are induced by the condensation of the counterions as depicted in the top panel. The color code for the various beads is the same as that in Fig. 1.

enhances the electrostatic repulsion between the surfactant head groups and makes the saddle geometry energetically unfavorable. Furthermore, as inferred from Figs. 3(a) and 3(b), a larger number of Sal^- ions interdigitate among the surfactant molecules within the branched portion as compared to those in spherical and cylindrical regions. Hence, the additional electrostatic repulsion facilitated by this increase in counterion condensation at the micelle-water interface compounds the unfavorable curvature energy of the saddles. Consequently, the branches are inherently unstable and incessantly move along the micelle contour as visualized in the Supplemental Material [27:S1] for $c_D = 0.3$ and $R = 0.8$. Quantitatively, the branch shown in the movie moves ~ 10 nm in 50 ns. We tracked the potential energy (PE), which is the sum of the nonbonded interaction energy among all the CG beads within the branched structure, associated with this motion during which counterions continually dissociate from and associate with the structure. As shown in Fig. 3(c), the net effect of such local concentration fluctuations is a reduction in the PE along the direction of sliding. We note that fluctuations in counterion

concentration could render a given sliding path energetically unfavorable, resulting in a reversal in the direction of branch motion. The persistence time of the sliding motion along a given direction is on the order of 10 ns.

B. Pathways of branch formation

From MD simulations, numerous pathways of branch formation were identified including those involving multiple linear and/or branched micelles resulting in a variety of micelle morphologies.

We show a few pathways of branch formation in Fig. 4, summarized as follows. (i) A kink in a wormlike micelle grows to a *Y-shaped* structure. (ii) Three micelles form a triple junction by losing their end caps, and further coarsening results in a branched structure. (iii) A nonuniform density of condensed counterions along a micelle surface creates special points which merge with the end cap of another micelle to form a branch. (iv) An *X-shaped* micelle forms by the coalescence of a cylindrical micelle and a branched micelle. (v) Surfactant exchange from the cylindrical portion of two micelles forms an *H-like* junction and is similar to the *ghostlike* crossing mechanism proposed by Appell *et al.* [5].

C. Branching and stress relaxation

To investigate the influence of micelle branching on stress relaxation, we study the transient response of micellar solutions after the cessation of a uniaxial extensional flow at various surfactant concentrations: $c_D = 0.2M$ and $0.3M$ for $R = 0.6$ and 0.8 . We consider microstructures shown in Figs. 5(a)(i) and 5(a)(ii) and 5(b)(i) and 5(b)(ii) which clearly indicate an increase in the number of branch points N_b with increasing R . Furthermore, the number of branch points also increases with increasing surfactant concentration c_D at a given R . A large N_b should then decrease the solution viscosity [14] as a consequence of the enhanced diffusion of branch points. Therefore, one would expect a direct dependence of stress relaxation and molecular diffusion on the degree of micelle branching. To test this hypothesis, we compute the viscosity $\eta(t)$ for solutions with varying degrees of branching [Figs. 5(a)(iii) and 5(b)(iii)] from the stress-autocorrelation function $\eta(t) = \frac{V}{k_B T} \sum_{i,j} \int_0^\infty dt \langle p_{ij}(t) p_{ij}(0) \rangle$ with $i \neq j = x, y, z$, where V is the system volume, k_B is

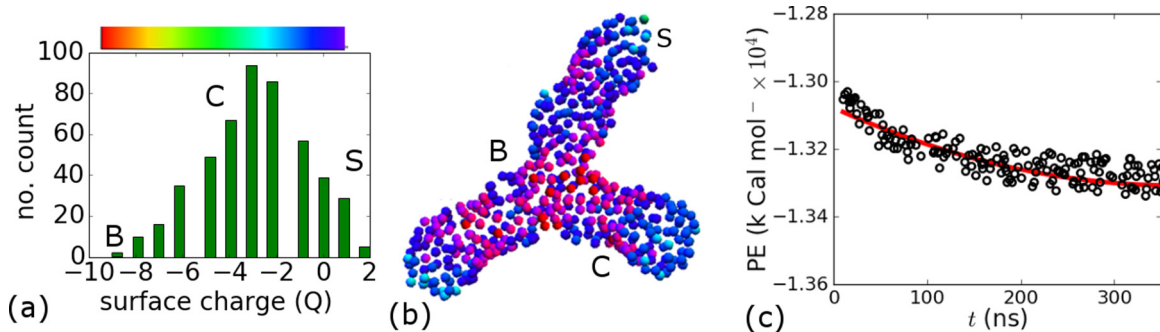


FIG. 3. Charge distribution and energetics of a branched micelle obtained from equilibrium simulations at $c_D = 0.3M$ and $R = 0.8$. (a) Distribution of net charge $Q = \sum q_i$ over the micelle surface. The color map corresponds to the Q values of the abscissa. Labels: S (spherical); C (cylindrical); and B (branch point). (b) Micelle surface color coded with Q values. (c) The potential energy of a branched micelle as a function of time associated with the sliding motion.

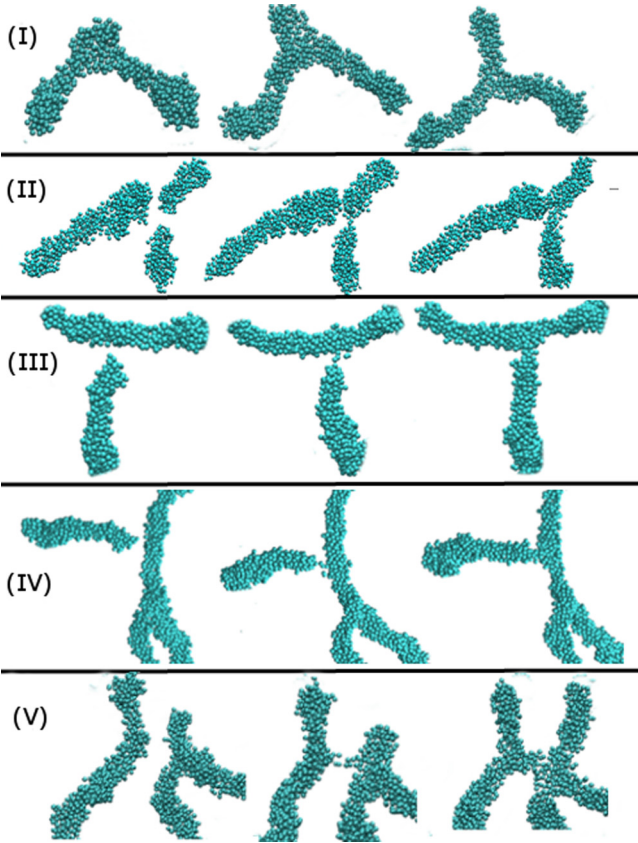


FIG. 4. Pathways of branch formation.

the Boltzmann constant, and T is the temperature. As shown in Figs. 5(a)(iii) and 5(b)(iii), the zero-shear viscosity η_0 , which is the plateau in $\eta(t)$, decreases with increasing N_b in accordance with previous studies [8,9,11]. To understand the underlying mechanism for this reduction in viscosity and the role of branching on stress relaxation, we study how an externally imposed stress relaxes in such systems. Towards this end, we deform the microstructures under a uniaxial tensile

strain at a constant strain rate in the x direction with zero pressure in y and z . Such a flow stretches the microstructure in the x direction whereas shrinks it in the other two directions [14]. In all of the simulations, the applied deformation is such that the equilibrium structures are stretched appreciably but yet retained their original topologies. In Figs. 5(a)(iv) and 5(b)(iv), we plot the residual stress $\sigma_{xx}(t)$ after the cessation of extensional flow. In all cases, stress decreases exponentially $\sigma_{xx}(t) \sim \sigma_{xx}(0)e^{-\alpha t}$. We observed the following exponents at various concentrations: (a) $\alpha = 0.05$ and 0.17 for $R = 0.6$ and 0.8 , respectively, at $c_D = 0.2M$ and (b) $\alpha = 0.10$ and 0.18 for $R = 0.6$ and 0.8 , respectively, at $c_D = 0.3M$. Clearly, stress relaxation is faster in a solution with a higher degree of branching. Closer inspection of the individual micelles in the simulations reveals that the branches indeed slide along the main chain as conjectured by Appell *et al.* [5]. This paper provides clear evidence that such sliding motion helps heal stresses imposed on the system.

D. Anomalous diffusion of surfactants

Ensemble-averaged (EA) MSD of different molecules and ions for $c_D = 0.1M$ and $R = 0.2$ is shown in Fig. 6. Diffusion of the entire system is approximately Gaussian ($\beta \sim 0.98$) whereas those of the surfactants and Sal^- counterions are subdiffusive ($\beta \sim 0.74$) which is consistent with the notion that they constitute the self-assembled micellar structure. However, persistent branch motion as well as breakage and recombination of micelle fragments could result in marked differences in the dynamics at the single molecule level. In order to probe such dynamic heterogeneity, we analyze the time-averaged (TA) MSD of the individual surfactants defined as

$$\langle r^2(\Delta) \rangle = \frac{1}{T - \Delta} \int_0^{T-\Delta} [\mathbf{r}(t + \Delta) - \mathbf{r}(t)]^2 dt, \quad (4)$$

where $\mathbf{r}(\mathbf{x}, \mathbf{y}, \mathbf{z})$ is the position vector of the surfactant center of mass and Δ and T are the lag time and total measurement time, respectively. In all calculations reported here, $T > 200$ ns. We show the TA MSD of representative surfactant molecules

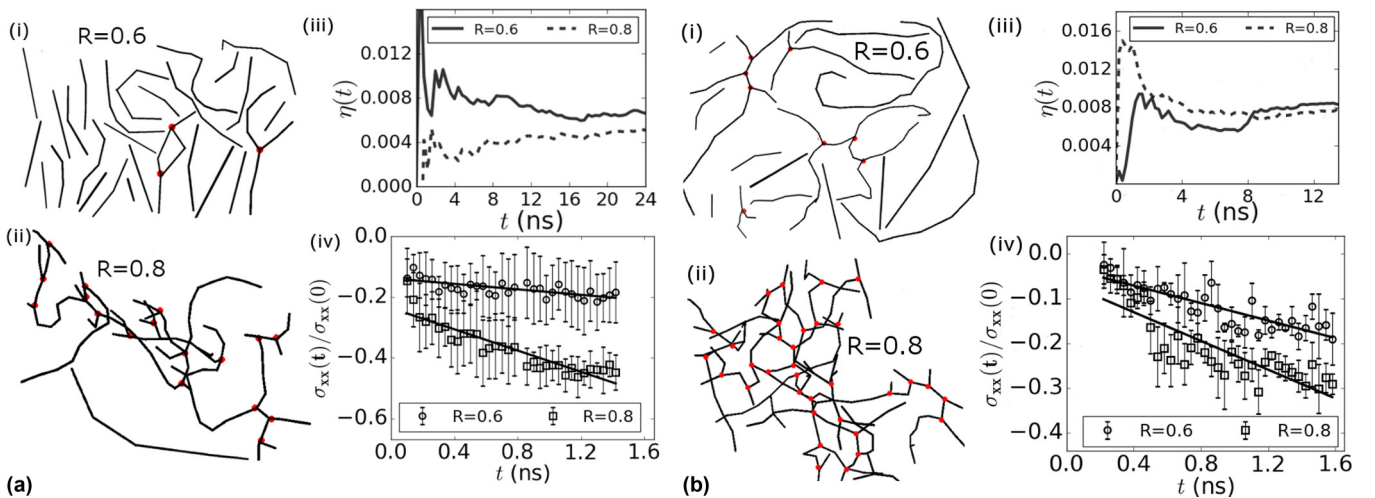


FIG. 5. Stress relaxation simulations. (a) $c_D = 0.2M$. (b) $c_D = 0.3M$. (i) and (ii) Microstructures at different R values. (iii) Viscosity η as a function of time for different concentrations. (iv) Time evolution of stress at different salt and surfactant concentrations after the cessation of an imposed extensional deformation (semilog y plot).

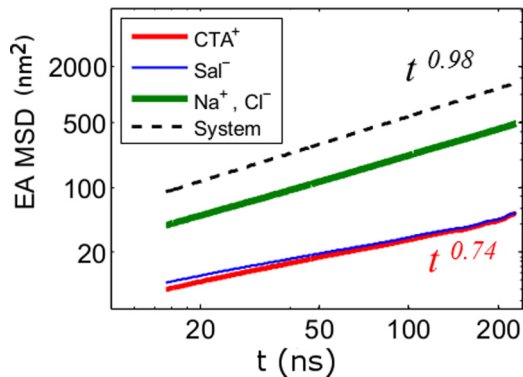


FIG. 6. EA MSD for different molecules and ions in a solution for $c_D = 0.1M$ and $R = 0.2$ (log-log plot).

at various surfactant concentrations and $R = 0.2, 0.4,$ and 0.8 in Fig. 7 along with the topological representations of the corresponding microstructures (top row) constructed by juxtaposing the three-dimensional micelle contour onto a two-dimensional plane. The branch points are denoted by red dots. The TA MSD plots show wide variation in surfactant dynamics with a broad distribution in the exponent, i.e., $0 \leq \beta \leq 2$. Subdiffusive motion results from the trapping

of micelles in locally crowded environments and persists at all concentrations. On the other hand, the mechanism underlying superdiffusive motion is concentration dependent. The MD trajectory of a surfactant molecule exhibiting superdiffusive motion [corresponding to the topmost TA MSD plot in Fig. 7(a)] is illustrated with red colored beads in the Supplemental Material [27:S2]. A closer inspection reveals that the corresponding micelle undergoes frequent recombination and breakage with the surrounding micelles. These observations indicate that superdiffusive motion in a dilute solution arises primarily due to transient combination and breakage of micelles. At intermediate concentrations [Fig. 7(b)], micelles are relatively longer, and reptation of micelle chains dominates the stress relaxation process. However, recombination and breakage still occur among shorter micelles. The TA MSD of a surfactant molecule that belongs to a shorter micelle entrapped in entanglements [signified by the plateau regions in Fig. 7(b)] exhibits superdiffusive behavior when the topological constraints are released and the micelle escapes the trap branched structures from upon further increasing R . A few examples of the TA MSD plots of individual surfactant molecules at $R = 0.8$ are shown in Fig. 7(c). We often observe superdiffusive behavior of surfactants belonging to one of the branches of a micelle as shown in the Supplemental Material [27:S3] [the red colored

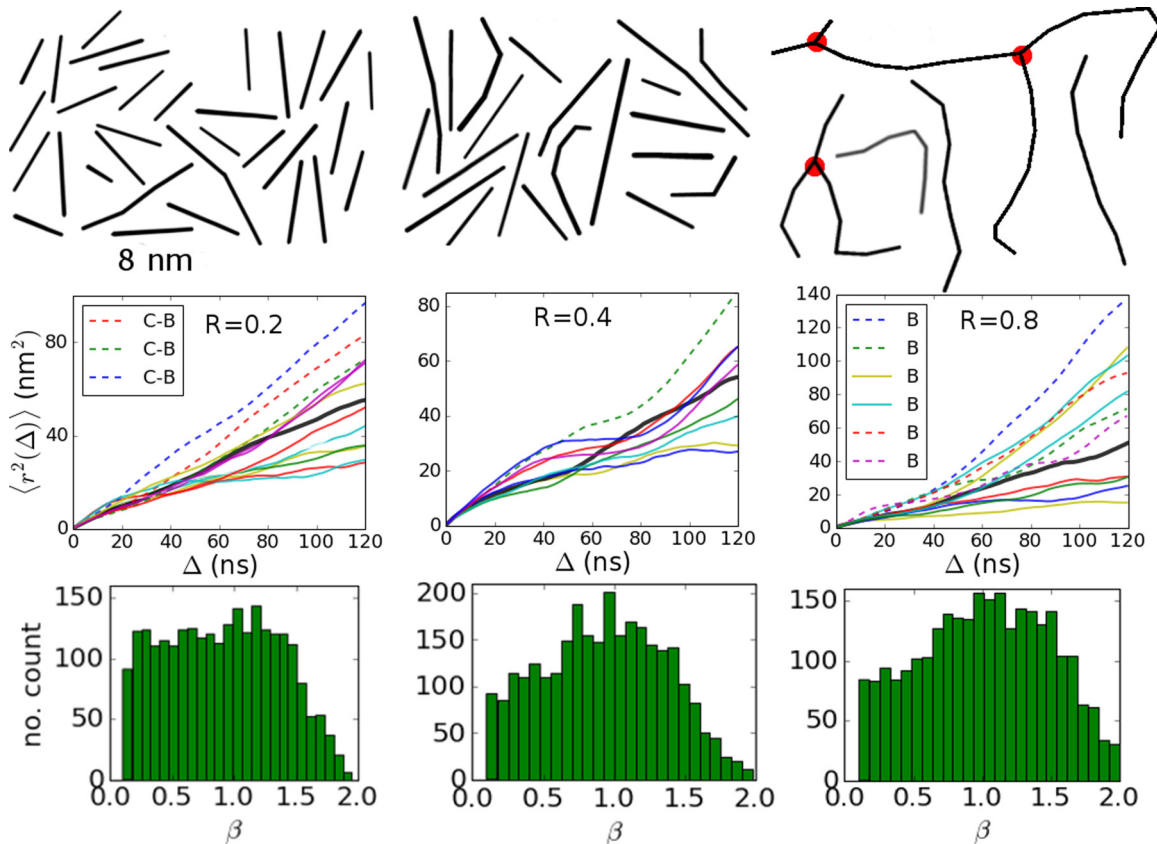


FIG. 7. First row: Microstructures for $R = 0.2, 0.4,$ and 0.8 at $c_D = 0.1M$. The number of branch points increases with increasing R as shown by the solid circles. Second row: TA MSD of representative surfactants showing normal, subdiffusive, and superdiffusive motions. (C-B): TA MSD of individual surfactant molecules in the solution belonging to a micelle that either combines with another micelle or breaks apart into two micelles. (B): TA MSD of individual surfactant molecules belonging to a branched micelle. Thick solid lines (black) represent normal diffusion, i.e., $\langle r^2(\Delta) \rangle \sim t$. Third row: Distribution of the diffusion exponent β .

beads represent the surfactant corresponding to the topmost plot in Fig. 7(c)]. It illustrates that superdiffusion also stems from the sliding motion of micelle branches. Diffusion in a micellar fluid occurs by solvent-mediated exchange of free surfactants, recombination and breakage of micelles, sliding motion of micelle branches, and reptation. Reptation inhibits free diffusion of molecules whereas micelle combination and sliding motion of branches enhance diffusion. Furthermore, the distributions of exponent β shown in the bottom row of Fig. 7 show that the number of surfactants exhibiting superdiffusive behavior increases with increasing R . This is consistent with the notion that branch motion as well as combination and breakage of micelles synergistically boost surfactant diffusion at higher R , whereas combination and breakage are the primary mechanism of superdiffusion at lower R .

IV. CONCLUSIONS

In conclusion, we have explored the dynamics of surfactant molecules in micellar solutions with diverse morphologies. Simulations have revealed multiple pathways of branch formation and provided direct visualizations of the sliding motion of micellar branches. We also have identified the energetic driving forces that induce incessant branch motion arising from an

excess counterion condensation at the branch points. Overall, diffusion of surfactant molecules within a micelle solution is strikingly heterogeneous as signified by the existence of a broad range of subdiffusive, normal, and superdiffusive space-time trajectories. Superdiffusion of surfactant molecules can arise from three mechanisms: sliding motion of branches along the micelle contour, breakage and recombination of micelle fragments, and ballistic motion of short micelles that escape from topological constraints. The latter mechanism is supported by FRAP measurements [18]. Finally, the CGMD simulations have provided clear evidence to validate a hypothesis that was put forward almost three decades ago that an increase in branch density facilitates faster stress relaxation in micellar fluids.

ACKNOWLEDGMENTS

This work used the computational resources provided by Extreme Science and Engineering Discovery Environment (XSEDE), which is supported by National Science Foundation Grant No. OCI-1053575. The authors acknowledged financial support from the National Science Foundation under Grants No. 1049489 and No. 1049454.

-
- [1] P. Debye and E. Anacker, *J. Phys. Chem.* **55**, 644 (1951).
 [2] D. Danino, Y. Talmon, H. Levy, G. Beinert, and R. Zana, *Science* **269**, 1420 (1995).
 [3] F. Lequeux, *Curr. Opin. Colloid Interface Sci.* **1**, 341 (1996).
 [4] M. Cates and S. Candau, *J. Phys.: Condens. Matter* **2**, 6869 (1990).
 [5] J. Appell, G. Porte, A. Khatory, F. Kern, and S. J. Candau, *J. Phys. II France* **2**, 1045 (1992).
 [6] A. V. Sangwai and R. Sureshkumar, *Langmuir* **27**, 6628 (2011).
 [7] A. Sambasivam, A. V. Sangwai, and R. Sureshkumar, *Phys. Rev. Lett.* **114**, 158302 (2015).
 [8] S. Dhakal and R. Sureshkumar, *J. Chem. Phys.* **143**, 024905 (2015).
 [9] S. A. Rogers, M. A. Calabrese, and N. J. Wagner, *Curr. Opin. Colloid Interface Sci.* **19**, 530 (2014).
 [10] Z. Lin, *Langmuir* **12**, 1729 (1996).
 [11] D. Sachsenheimer, C. Oelschlaeger, S. Müller, J. Küstner, S. Bindgen, and N. Willenbacher, *J. Rheol.* **58**, 2017 (2014).
 [12] D. Gaudino, R. Pasquino, and N. Grizzuti, *J. Rheol.* **59**, 1363 (2015).
 [13] S. May, Y. Bohbot, and A. Ben-Shaul, *J. Phys. Chem. B* **101**, 8648 (1997).
 [14] S. Dhakal and R. Sureshkumar, *ACS Macro Lett.* **5**, 108 (2015).
 [15] M. Lopez-Gonzalez, W. Holmes, and P. Callaghan, *Soft Matter* **2**, 855 (2006).
 [16] R. Angelico, U. Olsson, G. Palazzo, and A. Ceglie, *Phys. Rev. Lett.* **81**, 2823 (1998); R. Angelico, A. Ceglie, U. Olsson, and G. Palazzo, *Langmuir* **16**, 2124 (2000); R. Angelico, A. Ceglie, U. Olsson, G. Palazzo, and L. Ambrosone, *Phys. Rev. E* **74**, 031403 (2006).
 [17] R. Ganapathy, A. Sood, and S. Ramaswamy, *Europhys. Lett.* **77**, 18007 (2007).
 [18] A. Ott, J. P. Bouchaud, D. Langevin, and W. Urbach, *Phys. Rev. Lett.* **65**, 2201 (1990).
 [19] M. Silvander, G. Karlsson, and K. Edwards, *J. Colloid Interface Sci.* **179**, 104 (1996).
 [20] S. Candau and R. Oda, *Colloids Surf. Physicochem. Eng. Aspects* **183**, 5 (2001).
 [21] L. Ziserman, L. Abezgauz, O. Ramon, S. R. Raghavan, and D. Danino, *Langmuir* **25**, 10483 (2009).
 [22] D. Winter, J. Horbach, P. Virnau, and K. Binder, *Phys. Rev. Lett.* **108**, 028303 (2012).
 [23] X.-L. Wu and A. Libchaber, *Phys. Rev. Lett.* **84**, 3017 (2000).
 [24] S. Hild, T. Fukuhara, P. Schauß, J. Zeiher, M. Knap, E. Demler, I. Bloch, and C. Gross, *Phys. Rev. Lett.* **113**, 147205 (2014).
 [25] S. Plimpton, *J. Comput. Phys.* **117**, 1 (1995).
 [26] S. J. Marrink, H. J. Risselada, S. Yefimov, D. P. Tieleman, and A. H. de Vries, *J. Phys. Chem. B* **111**, 7812 (2007).
 [27] See Supplemental Material at <http://link.aps.org/supplemental/10.1103/PhysRevE.96.012605>, showing a typical example of branch motion along the contour of the main chain of a branched micelle (S1), for transient combination and breakage of micelles that contribute to the superdiffusive motion (S2), and for the superdiffusive motion arising due to the sliding motion of a micelle branch (S3).